研究論文

Experimental Observation of Bifurcation Nature of Radial Electric Field in CHS Heliotron/Torsatron

FUJISAWA Akihide, IGUCHI Harukazu, YOSHIMURA Yasuo, MINAMI Takashi, TANAKA Kenji, OKAMURA Shoichi, MATSUOKA Keisuke and FUJIWARA Masami
National Institute for Fusion Science, Toki 509-5292, Japan

(Received 19 January 1999 / Accepted 8 March 1999)

Abstract

Several interesting phenomena, such as the formation of a particular potential profile with a protuberance around the core and oscillatory stationary states termed *electric pulsation*, have been discovered using a heavy ion beam probe in the electron cyclotron heated plasmas of the CHS. This paper presents experimental observations which indicate that bifurcation of the radial electric field is responsible for such phenomena; existence of an ECH power threshold to obtain the profile with a protuberance, and its striking sensitivity to density. In particular, flip-flop behavior of the potential near the power threshold clearly demonstrates bifurcation characteristics. Bifurcation of radial electric field in neoclassical theory is presented, and its qualitative expectation is discussed in the bifurcation phenomena. The neoclassical transition time scale between two bifurcative states is compared with the experimental observations during the electric pulsation. It is confirmed that the neoclassical transition time is not contradictory with the experimental one.

Keywords:
toroidal helical plasma, CHS, electric field bifurcation, HIBP, protuberance potential profile, power threshold, flip-flop behavior, repetitive transition oscillatory steady state, neoclassical theory

1. Introduction

Toroidal helical devices are one of the candidates for a magnetic confinement fusion reactor. In contrast to tokamaks, the toroidal helical devices have a rotational transform in their vacuum magnetic field. This feature gives an attractive advantage that a disruption-free steady state is easily realized. However, the favorable property of the magnetic field causes the other characteristics that have never been seen in axisymmetric devices such as tokamaks. In other words, the magnetic field of toroidal helical devices inherently possesses helical inhomogeneity in addition to toroidicity.

A disadvantage is that the inhomogeneity (or helical ripple) enhances collisional heat and particle transports. The helical ripple transport is, however, strongly affected by the internal radial electric field. The transport of toroidal helical devices could be controlled by managing the radial electric field [1,2]. The theory has also predicted that toroidal helical plasmas can show bifurcation in radial electric field if the plasma is in a certain parameter regime. These bifurcation characteristics should be an important factor to determine the static structure and temporal behavior of the toroidal helical plasma. The radial electric field is an important physical quantity to be investigated in the toroidal helical plasma.

A heavy ion beam probe (HIBP) [3,4] has been

corresponding author's e-mail: fujisawa@nifs.ac.jp
† この論文は第14回年会にて招待講演として発表されたものを論文化したものです。

installed on the Compact Helical System (CHS), a toroidal helical device, to investigate electrostatic potential of interior. The elaborate measurements of the HIBP have revealed many unique features of toroidal helical plasmas. In particular, various findings have been obtained in electron cyclotron heated (ECH) plasmas with on-axis resonance, such as a potential profile with a protuberance, transition between branches of bifurcation and oscillatory steady states. These phenomena should be associated with the neoclassical bifurcation of the radial electric field.

This paper presents several interesting observations with the HIBP in ECH plasmas of CHS. We describe several properties of a potential profile with a protuberance, and then introduce two examples of oscillatory stationary states of electric pulsation. A neoclassical calculation for a phase diagram of radial electric field is presented to show its bifurcation property, and to discuss theoretically expected features for the bifurcation phenomena. A rough comparison between the theory and the experiment is made in the transition times between bifurcative states. It is shown that the neoclassical theory is sufficient to explain the order of the transition time scale.

2. Experimental Set-up

The CHS is a medium size heliotron/torsatron device; the major and minor radii are 1.0 m and 0.2 m, respectively [5]. The device has a pair of helical winding coils and four pairs of poloidal coils to control the position and shape of the plasma. The magnetic field configuration has a periodicity of $l = 2$ and $m = 8$ in poloidal and toroidal directions, respectively. The CHS has co- and ctr-injection lines of neutral beams, and three gyrotrons; two of 53.2 GHz and one of 106 GHz.

The CHS has an HIBP [3,4] in order to measure the structure of potential and its temporal behavior. The HIBP has excellent temporal and spatial resolutions, that are very powerful for investigating fast time scale phenomenon. The HIBP has a unique feature in that the beam sweep system is installed on the analyzer side as well as on the injection side. Using this method, 'active trajectory control' [6], the accessible region of plasmas is extended widely for several different configurations.

The observation location of the HIBP can be altered by managing sweep voltages to control the beam trajectory. The experiments we will present here are performed on the magnetic field configuration whose axis is located at $R_{ax} = 0.921$ m and the strength at the center is 0.88 T. In this configuration, the required beam energy is 72 keV when cesium is used, and an almost full radial scan is possible. The HIBP can be operated in two ways; radial scan mode to investigate time evolution of the potential profile, and a fixed sweep mode to investigate fast time scale phenomena with a frequency resolution of up to 450 kHz.

3. Experimental Observations

3.1 Bifurcation nature in potential profiles

One of the particular results is a recent finding of a potential profile with a *protuberance*. When rather strong ECH power is applied, the potential profile exhibits a prominent peak around the core region. The experiments to date have confirmed existence of an ECH power threshold to obtain this protuberance. Figure 1 shows the dependence of the shape of the potential profile of hydrogen plasmas on ECH power. The potential profiles were obtained in sequential shots. The line averaged electron density of this case is $n_e \simeq 4 \times 10^{12}$ cm^{-3}. The profile of 130 kW (squares) just shows a simple feature of a parabolic profile. As ECH power increases up to 150 kW (open circles), the profile abruptly changes to acquire the unique feature of a protuberance. The feature is lost again by increasing the ECH power. The profile with a protuberance is obtained

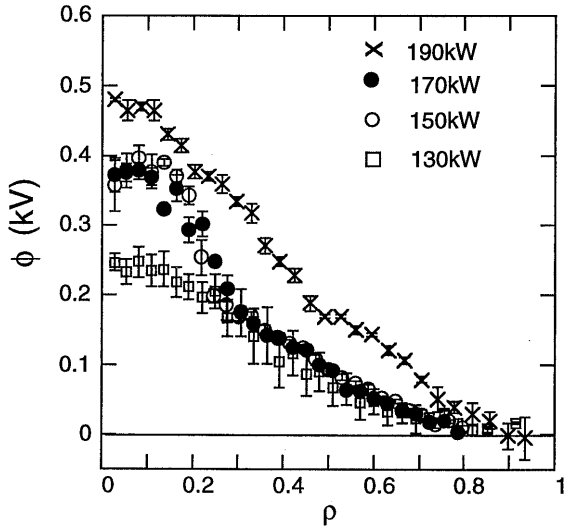

Fig. 1 Dependence of potential profile on ECH power. A threshold is shown to form a potential profile with a protuberance. The square, open circles, closed circles and x-marks represent the potential profiles with ECH power of 130 kW, 150 kW, 170 kW and 190 kW, respectively.

in a certain window of ECH power for a fixed density.

The protuberance profile shows a spatial *discontinuity* of radial electric field at $\rho \sim 0.3$, where ρ is the normalized minor radius. The HIBP measurements in another experiment indicate that the radial electric field varies from 8 kV/m to 2 kV/m across the transient layer whose width is estimated at approximately 1 cm. The plasma rotation of $E \times B$-velocities drastically changes through this layer. Hence, the layer should work as a momentum transport barrier. Recently, it has been confirmed that the point actually plays a role as an internal transport barrier for electron energy [7]. Thomson scattering measurements also show a steep gradient of electron temperature at the point, that leads to a high central electron temperature of ~ 2 keV. An electron energy (and momentum) transport barrier is established at $\rho \sim 0.3$.

The temporal behavior at the power threshold manifests the bifurcation nature of the protuberance profile more clearly. Figure 2 shows the time evolution

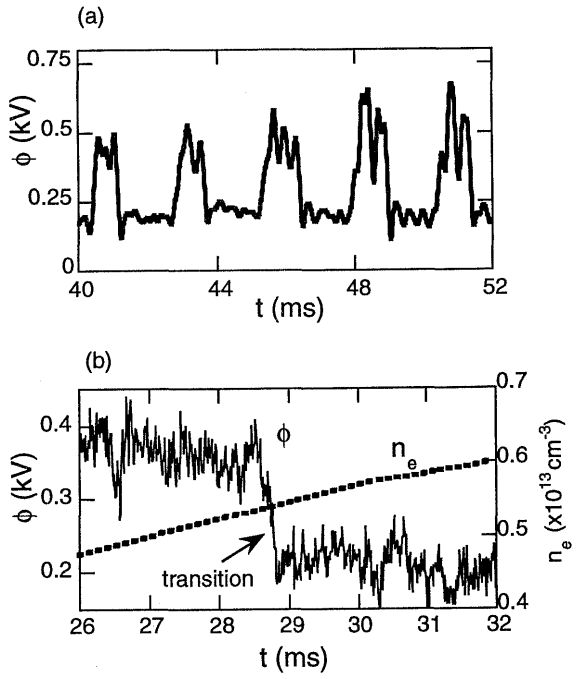

Fig. 2 (a) Time evolution of central potential when the ECH power is near the threshold. The flip-flop pattern of the waveform clearly demonstrates a bifurcative nature in the protuberance potential. (b) A time evolution of central potential (solid line) and line-averaged density (dashed line) with the ECH power of 200 kW. At a critical density, the plasma potential makes the transition from the protuberance profile to a parabolic profile.

of the central potential of a deuterium plasma with only ECH heating whose power is on the threshold (~ 150 kW). The waveform exhibits *flip-flop* behavior; the potential takes higher and lower values alternately for approximately 2 ms. The higher and lower potential states correspond to the potential profiles with and without a protuberance in Fig. 1, respectively. In other words, the plasma goes back and forth between the two distinctive profiles. No special magnetic activity has been detected before the creation and annihilation of the protuberance.

The protuberance feature has a great sensitivity to density as well as the ECH power. An example is demonstrated in Fig. 2(b). This is a hydrogen plasma which is also maintained with only ECH heating at a power of 200 kW. The density gradually increases toward the end of the discharge. In the early stage of the discharge, the potential profile has the protuberance. However, when the density reaches a critical value of $n_e \simeq 5 \times 10^{12}$ cm^{-3}, the potential suddenly decreases in a dozen microseconds time scale. The plasma loses the protuberance, and goes to the simple parabolic profile while the density changes by $\Delta n_e/n_e \simeq 0.5\%$ or $\Delta n_e \sim 2 \times 10^{10}$ cm^{-3} owing to its gradual increase. It can be interpreted as two equilibrium potential profiles (see Fig. 1) which can exist at one density value. This waveform shows the transition between these two profiles. This discontinuous change of potential profile to density also indicates that the ECH plasma has the bifurcation nature in potential or radial electric field.

3.2 Electric pulsation

The previous flip-flop pattern has the same lifetime for both lower and higher potential states. As the ECH power (or density) changes, the plasma shows other interesting patterns. Here, we present two examples of time evolution of potential when the power is fairly above the threshold (~ 300 kW). This phenomenon has been already reported in Ref. [8], being referred as *electric pulsation.*

In these two examples, the plasma was initially sustained with neutral beam injection (NBI), then the ECH was applied. Figure 3(a) shows the first example of the electric pulsation observed in the potentials at the center and an outer radius, together with the time evolution of the line-averaged electron density. After the ECH is on at $t \simeq 45$ ms, the electron density decreases and relaxes to a steady state of $n_e \simeq 4 \times 10^{12}$ cm^{-3} approximately in 5 ms. The Thomson scattering measurement implied that the electron temperature was

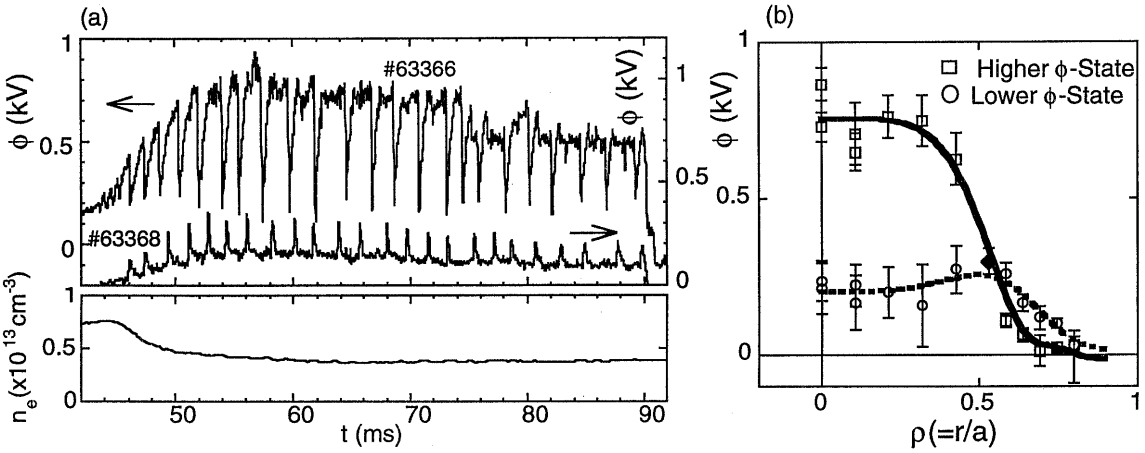

Fig. 3 (a) Pulsating behavior of the potentials at the center and at an outer radius of ρ = 0.59 in CHS plasmas. This phenomenon is referred to as electric pulsation. The example is observed in a combined ECH+NBI heating phase. The time evolution of the line averaged electron density, that was measured with an HCN interferometer, is shown below. (b) The potential profiles of higher and lower potential states. Here ρ is the normalized minor radius.

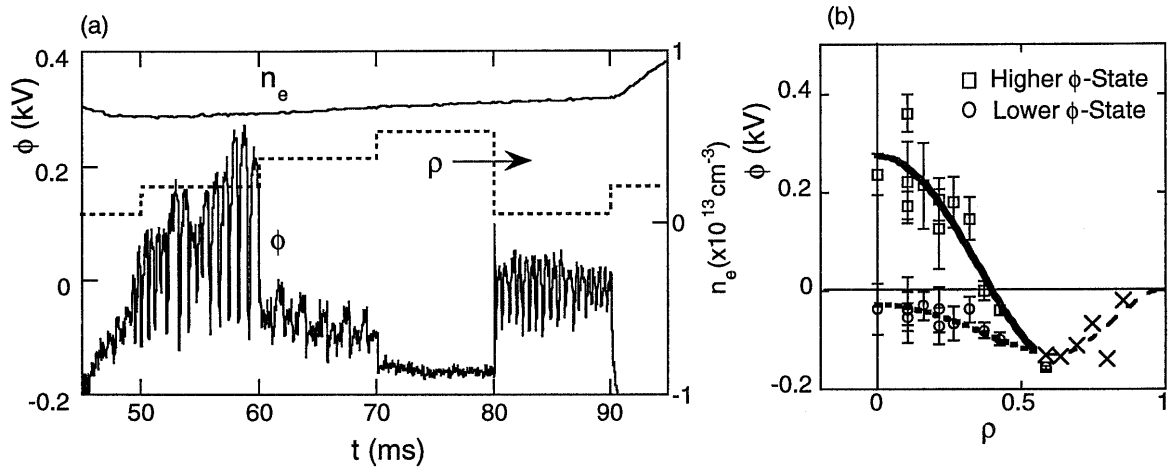

Fig. 4 Another example of long-term electric pulsation. In this case, the electron density is rather higher about $n_e = 7 \times 10^{12}$ cm^{-3}. (a) Time evolution of potential near the center (solid) and line averaged electron density (dashed-dotted line). The observation point of the HIBP, as is shown by the dashed line, is altered step by step in every 10 ms. (b) Potential profiles of higher and lower potential states. Outside of ρ = 0.57, no change is seen during the pulsation. The data represented by the x-marks are taken in a radial scanning mode.

~ 1 keV, although the scattering light was poor in this case. The potential goes to an oscillatory steady state, where negative pulses of potential by –0.6 kV occur quasi-periodically in every 2 ms near the plasma core. On the other hand, the potential outside of ρ = 0.53 shows quasi-periodic positive pulses with the same interval as the center.

In contrast to the flip-flop pattern, the higher potential state has a longer lifetime than that of the lower one. Figure 3(b) shows potential profiles of these two states. The plasma swings repeatedly between these quite different profiles. The difference in shape is much larger than that of the flip-flop pattern. The change of potential profiles is more global.

As the density increases, the pulsation characteristics alter. Figure 4(a) demonstrates the time

evolution of the central potential and the line-averaged electron density. In this case, the line-averaged electron density in the oscillatory steady state is $n_e \sim 7 \times 10^{12}$ cm^{-3}. The central potential at the higher potential state is 0.3 ~ 0.4 keV. Being different from the case of Fig. 3(a), the observation point of HIBP is altered step by step every 10 ms; $\rho = 0.21$ (50–60 ms), $\rho = 0.37$ (60–70 ms), $\rho = 0.53$ (70–80 ms) and $\rho = 0.05$ (80–90 ms). No pulse can be seen in the step of $\rho = 0.53$, while pulsating behavior is still observed in the following step of $\rho = 0.05$. This fact shows that the pulsation occurs inside of $\rho \sim 0.5$.

In this oscillatory state, the central potential gradually decreases. The change is ascribed to the gradual development of bulk plasma parameters, which are represented by the electron density. The potential at the higher state in the period of $t = 80$ ms to $t = 90$ ms is lower than that of $t = 50$ ms to $t = 60$ ms. In these two periods, the frequency of the later phase (~ 1.5 kHz) is higher than that of the earlier phase (~ 1.0 kHz). A statistical analysis shows that the pulsation amplitude becomes smaller with density increase.

Figure 4(b) shows the profiles of higher and lower potential states for the case of Fig. 4(a). Each point data is taken in the period from $t = 50$ ms to $t = 70$ ms to avoid changes due to bulk parameter differences. In this example, the potential shapes of two bifurcative states are clearly different from those of the previous case in Fig. 3. The plot clearly demonstrates that the pulsation occurs inside of $\rho = 0.5 \sim 0.6$, and the change of central potential is about 0.3 kV. The potential outside of $\rho = 0.5 \sim 0.6$ (x-marks) shows no change during the pulsation; the data of these locations is taken in the radial scan mode. The potential profiles swing repeatedly between two 'Mexican hat profiles' with higher and lower *domes* during the pulsation.

In the case of Fig. 3, it has been found that profiles of electron temperature and density change are clearly correlated with potential pulsation. There, the observation shows that the plasma loses 5% of its internal energy when the plasma goes to the low potential state; the internal plasma energy is about 400 J (corresponding to an average $\beta \sim 0.2\%$). Clear correlation of the potential pulse with Hα also demonstrates that the effect of pulsation reaches the plasma periphery. However, in the case of Fig. 4, the effects of pulsation are limited within the narrower region around the core, since the Hα signal shows no clear correlated pulse.

So far we have several preliminary findings about the dependence of pulsation characteristics on density as follows. (1) As the density increases, the pulse amplitude becomes smaller and then the pulsation fades out above a critical density. (2) As the density decreases, the pulsation frequency becomes smaller. It is expected that finally the plasma may stay only in the higher potential state below a critical density. (3) The threshold power of ECH to induce the electric pulsation appears to be higher as the density increases. With an ECH input power of 200 kW, the electric pulsation cannot be seen when the electron density is above $n_e \sim 5 \times 10^{12}$ cm^{-3}. With an ECH input power of 300 kW, the critical density is $n_e \sim 8 \times 10^{12}$ cm^{-3}.

4. Comparison with Neoclassical Theory

4.1 Bifurcation characteristics in neoclassical theory

Experimental observations show the bifurcative nature of ECH plasmas. The neoclassical theory is the most accomplished one in its framework at present. The theory has described the highly nonlinear dependence of radial electric field on plasma parameters in the toroidal helical plasma .

An example of the neoclassical calculation is obtained using the Hastings formula [1,2]. The assumptions used in the present calculation are as follows; $B = 0.9$ T, $T_i(\rho) = 300$ eV, $Z_{eff} = 2$, $\partial \ln n_e(\rho)/\partial\rho = 0$ and $\partial \ln T_e(\rho)/\partial\rho = \partial \ln T_i(\rho)/\partial\rho = -1.1$. The ion species is assumed to be hydrogen. We choose $\varepsilon_h = 0.063$ and $\varepsilon_t = 0.16$, where ε_h and ε_t are the helical ripple coefficient and the toroidal coefficient (or inverse aspect ratio), respectively. These coefficients correspond to $\rho \simeq 0.5$ of the CHS plasma. The temperature gradients correspond to the value of a parabolic profile at $\rho = 0.5$. The assumed parameters are in a plausible range of the CHS experimental values. Under these assumptions, the balance of nonambipolar neoclassical fluxes, that is $\Gamma_i^{na}(E_r) = \Gamma_e^{na}(E_r)$, yields an electric field as a function of electron density and electron temperature. Figure 5(a) shows a calculation result in the n_e-T_e plane, and the crescent region which is outlined with a bold line indicates an area where multiple solutions exist. The contour of $E_r = 0$ is indicated by the bold dashed line, while other contours of constant electric field are also shown by thin dashed lines.

The radial electric field on a line crossing the crescent region shows bifurcation characteristics. The upper and lower boundaries correspond to bifurcation points from higher (H)- to lower (L)-branch, and/or

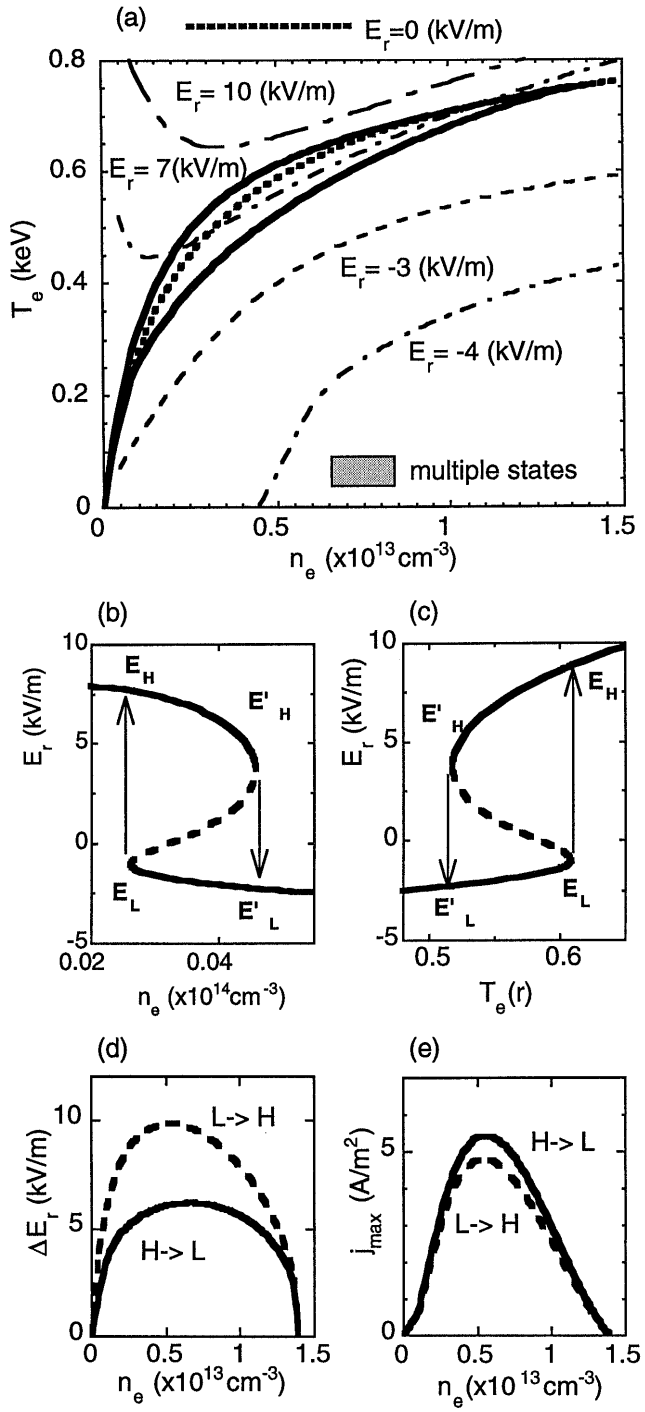

Fig. 5 An example of neoclassical calculation. The assumptions used in the calculation are $T_i(\rho)$ = 300 eV, Z_{eff} = 2, $\partial \ln n_e(\rho)/\partial\rho = 0$ and $\partial \ln T_e(\rho)/\partial\rho = \partial \ln T_i(\rho)/\partial\rho = -1.1$. We choose $\varepsilon_h = 0.063$ and $\varepsilon_t = 0.16$, which corresponds to $\rho \simeq 0.5$ of the CHS hydrogen plasma. (a) Region where multiple steady states exist in $n_e - T_e$ plane (shaded region). Contours of constant electric field are shown by dashed lines. (b) Bifurcation curve of radial electric field as a function of density. $T_e(\rho)$ = 0.5 keV is assumed. (c) Bifurcation curve of radial electric field as a function of temperature. $n_e(\rho) = 5 \times 10^{12}$ cm^{-3} is assumed. (d) Neoclassical maximum radial current during transition j_{max}. (e) Difference of radial electric field between two branches E_{gap}.

from L- to H-branch, respectively. Inside of the region surrounded by the boundaries, two stable and an unstable roots exist. Two examples of curves exhibiting such characteristics are presented in Figs 5(b) and 5(c). Figure 5(b) is the radial electric field as a function of electron density with $T_e = 0.5$ keV, and Fig. 5(c) is that as a function of electron temperature with $n_e = 5 \times 10^{12}$ cm^{-3}. Both curves have the bifurcation nature of the radial electric field.

From a theoretical point of view, it is necessary, therefore, for a spatial discontinuity of the radial electric field and for the transitions to occur that the plasma parameters at a certain radius should fall within the crescent regime in Fig. 5(a). In transition layer of the protuberance potential profile, two branches of radial electric field are considered to converge. The radial electric field inside the transition layer belongs to the H-branch of bifurcated states, while the radial electric field outside still remains in the L-branch.

The electric pulsation can be regarded as a limit cycle associated with the bifurcation curves, such as Figs. 5(b) or 5(c). If the plasma parameters at a radius are on a boundary of the crescent regime (or a bifurcation point in Figs. 5(b) or 5(c)), the transition spontaneously occurs in a faster time scale than confinement time scale. Then the transport alters, and the plasma parameters could change toward the other boundary in a confinement time scale. As soon as the plasma reaches the boundary, the transition happens to the other direction. In Figs. 5(b) or 5(c), the plasma is considered to go around the circuit surrounded by the points E'_H-E'_L-E_L-E_H. In this scenario, the pulsation frequency should be determined by the slow phases of E_H-E'_H or E'_L-E_L.

The other particular point to be mentioned is that the electric field is uniquely defined, as is shown in Fig. 5(a), above $n_e \sim 1.5 \times 10^{13}$ cm^{-3}. No bifurcation phenomenon, hence, is expected above the critical density. This feature should be associated with the experimental observation that the pulsation disappears above a critical density. In higher temperature and density, the width of the crescent regime becomes narrower. Therefore, it takes a shorter time that the plasma reaches the next bifurcation point. It is expected, thus, that the repetition frequency becomes higher as the density increases.

4.2 Transition time scales

A transition between these branches occurs if the plasma parameters are on boundaries of the crescent region in Fig. 5(a). During the transitions, the balance of nonambipolar fluxes is broken. Then the radial current flows proceeding the transition. The transition time can be predicted by neoclassical theory. The change in radial electric field obeys the following equation [9],

$$\varepsilon_\perp \varepsilon_0 \frac{\partial E_r}{\partial t} = -j_r(E_r). \qquad (1)$$

Here, $\varepsilon_\perp = (1 + 2q^2)(1 + c^2/v_A^2)$ is the perpendicular dielectric coefficient of plasma, where q, v_A and c are the safety factor, Alfvén and light velocities, respectively.

The radial current can be well expressed by a simple form as $j_r(E_r) \sim 4j_{max}\ (E_r - E_H)(E_r - E_L)/\Delta E_{gap}^2$ with $\Delta E_{gap} = E_H - E_L$ representing the difference in the electric field between the two branches, where j_{max}, E_H and E_L are the maximum radial current during the transition, and the values of radial electric field of high and low branches, respectively. Then the solution of Eq. (1) takes the form of $\tanh[(t - t_0)/\tau_{Neo}]$, where the time scale is represented by the constant $\tau_{Neo} \simeq \varepsilon_\perp \varepsilon_0 \Delta E_{gap}/2j_{max}$. Two quantities are necessary to estimate the transition time constant, ΔE_{gap} and j_{max}. These two values are plotted in Figs. 5(d) and 5(e) as a function of electron density along the boundaries of the crescent regime in Fig. 5(a).

As is already stated, each pulse in the electric pulsation can be regarded as a transition between two bifurcative states. Their time constants, which are an essential transition property, should be investigated in more detail. Figure 6 shows typical examples of backward (lower (L)- to higher (H)-potential state) and forward (H- to L-potential state) transitions near the plasma center from the previous two cases; (i) a pair of typical transitions in low density pulsation of Fig. 3(a) (ii) that in higher density of Fig. 4(a). The time evolution during transitions can be expressed by $\tanh[t/\tau]$-function. This functional form is used to estimate the characteristic time of the transition. The typical time constants of forward and backward transitions are a few tens of microseconds approaching a hundred microseconds. It is a common feature that the forward transition is faster than the backward one.

Figures 7 shows the comparison of experimental time constants of transitions with the neoclassically expected values; Figs. 7(a) and 7(b) are for the forward and the backward transitions, respectively. The closed circles represent the averages of the experimental constants in the plasma core for three points of the line-averaged density. The error bars of the data points

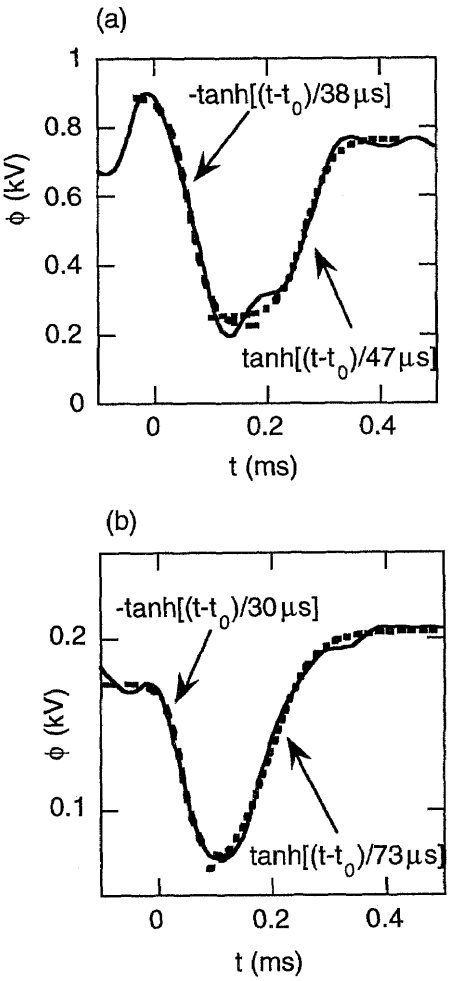

Fig. 6 Examples of transition waveforms in central potential. (a) Experimental time scale of transition that is observed in electric pulsation with low density in Fig. 3. (b) Experimental time scale of transition that is observed in electric pulsation with high density regime in Fig. 4.

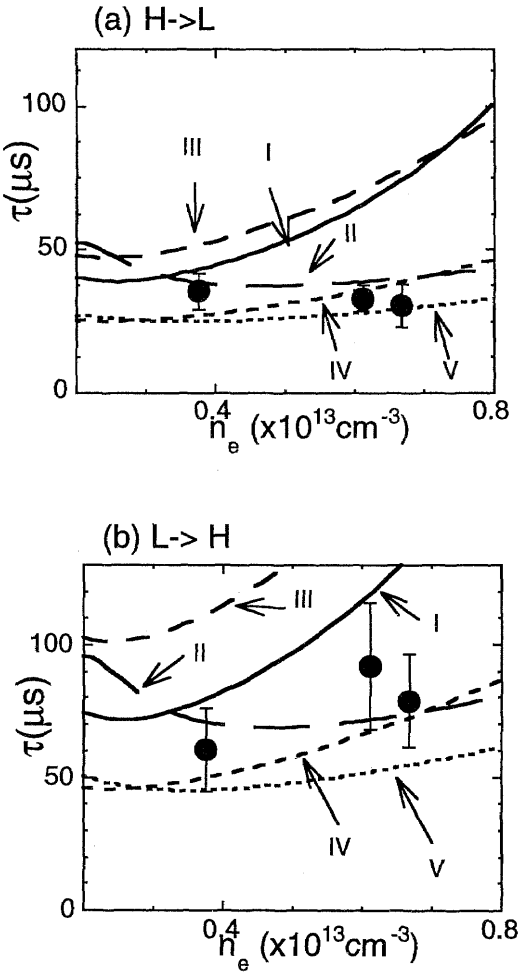

Fig. 7 Comparison of neoclassical transition time constants with the experimental ones at several density values. (a) Time constant for the forward transition. (b) Time constant for the backward transition. The closed circles represent the experimental values. The solid line indicates the theoretical values when the plasma parameters are assumed to be those of Fig. 5. The other lines are the theoretical values with different assumptions of the plasma parameters as are stated in the text.

indicate the standard deviation of the ensembles that consist of approximately more than a dozen transitions. The solid line represent the neoclassical constant that is estimated using plasma parameters in Figs. 5(d) and 5(e). In order to take experimental uncertainty of the plasma parameters into account, the other dashed lines in Figs. 7 indicate the neoclassical time constants using different assumptions. The parameters, $B = 0.9$ T, $Z_{eff} = 2$, $\varepsilon_t = 0.16$, $\partial \ln n_e(\rho)/\partial\rho = 0$, $\partial \ln T_i(\rho)/\partial\rho = -1.1$, are commonly assumed for all cases. The other parameters are assumed for five different cases as follows; (I) $T_i(\rho) = 300$ eV, $\partial \ln T_e(\rho)/\partial\rho = -1.1$, $\varepsilon_h = 0.063$, (II) $T_i(\rho) = 400$ eV, $\partial \ln T_e(\rho)/\partial\rho = -1.1$, $\varepsilon_h = 0.063$, (III) $T_i(\rho) = 300$ eV, $\partial \ln T_e(\rho)/\partial\rho = -3$, (IV) $T_i(\rho) = 300$ eV, $\partial \ln T_e(\rho)/\partial\rho = -1.9$, $\varepsilon_h = 0.092$, (V) $T_i(\rho) = 400$ eV, $\partial \ln T_e(\rho)/\partial\rho = -1.9$, $\varepsilon_h = 0.092$. Case (I) has the same parameters as those of Fig. 5. In cases (IV) and (V), the helical ripple coefficient corresponds to the value of $\rho = 0.6$, and the

electron temperature gradient is also the value of a parabolic profile at $\rho \simeq 0.6$.

As is shown in Figs. 7(a) and 7(b), the experimental time constants are in the range of the theoretical expectation within the present precision of the experiments. Both experimental and theoretical time constants have an agreement in the tendency that the backward transition time is slower than the forward one. It is worthwhile to note that the calculation is made for a local spatial point, although the actual transition during the pulsation is accompanied by a global structural change. Hence, the transition time constant is to be expected from the neoclassical calculation for the plasma core region, and the neoclassical particle flux imbalance could be a main contributor of the radial current inducing the transition.

5. Discussion and Conclusion

We have presented several interesting observations in ECH plasmas of CHS. As for the formation of a potential protuberance, the following bifurcation properties are presented. (1) There is an ECH power threshold for obtaining the potential protuberance. (2) The potential protuberance is lost, being remarkably sensitive to density. Moreover, the bifurcation characteristic is more clearly demonstrated in the flip-flop pattern near the power threshold. The waveform is interpreted as repetitive transitions between two bifurcative states, with both states being equally stable since both lifetimes are almost the same. The electric pulsation is a variation of this flip-flop pattern, where the higher potential state has a longer lifetime than that of the lower state. There the ECH power is well above the critical value, so that the higher potential state should be more stable.

The experimental observations presented here can be qualitatively understood by the neoclassical bifurcation nature of the radial electric field. The plasma parameter regime where the bifurcation phenomena occur is not contradictory to neoclassical expectation. The neoclassical time scale of the transition is of the same order of the observation. The plasma parameters are not measured with a sufficient accuracy to discuss detailed discrepancy with the theory. Our present conclusion is, therefore, that the phenomena are deeply connected to the bifurcation property as predicted by neoclassical theory, although future experimental observations may impose a modification on the neoclassical bifurcation property, by taking some other effects into account (*e.g.*, bipolar part of anomalous cross-field transport, loss-cone loss, Reynolds stress etc. [9]).

As for tokamaks, many bifurcation phenomena already have been reported, such as the formation of edge and internal transport barriers [10-12]. The most predominant hypothesis to explain the formation of both transport barriers is associated with a bifurcation of the radial electric field [13,14], and the resulting shear of the radial electric field suppressing the fluctuation driven transport [15-17]. It is an important future work to investigate similarities and differences between the the bifurcation phenomena observed in the toroidal helical plasmas and tokamaks. That will be useful for a systematic understanding of the structure or pattern formation of toroidal plasmas.

The electric pulsation is an oscillatory steady state, that is somewhat analogous to Edge Localized Modes (ELMs) in tokamaks [18,19]. Based on the analogy to ELMs, the phenomenon should be highly important for fusion applications. In the case of the electric pulsation in the low density regime, the particle is also swept out from the plasma, being correlated with each pulse. Therefore, the pulsation could be used for ash removal. In order to control this phenomenon, it is necessary to know the conditions under which the electric pulsation could occur in the plasma parameter regimes. This identification is also important to clarify the physical mechanisms of the pulsation.

In conclusion, we have described various spatial and temporal features of potential profiles that have been observed in ECH plasmas. The protuberance potential profile (or transport barrier) and an oscillatory steady state should be caused by the neoclassical bifurcative characteristic of the radial electric field. No serious discrepancy has been found with the neoclassical expectations within the present experimental precision. Particularly, the transition time scale between the bifurcative states is in the predictable range of neoclassical theory. The electric pulsation holds great importance for fusion application as well as for plasma physics. Further studies of these phenomena will be essential for complementary understanding of other bifurcation phenomena in tokamaks.

Acknowledgments

The authors are grateful to Dr. Y. Hamada, the CHS experimental group for their experimental support. One of the authors (A.F.) would like to give special thanks to Dr. H. Sanuki, Dr. K. Itoh and Dr. S.I-Itoh for their useful discussion and valuable comments.

References

[1] D.E. Hastings, W.A. Houlberg and K.C. Shaing, Nucl. Fusion **25**, 445 (1985).

[2] L.M. Kovrizhnykh, Nucl. Fusion **24**, 435 (1984).

[3] F.C. Jobes and R.L. Hickok, Nucl. Fusion **10,** 195 (1970).

[4] G.A. Hallock, J. Mathew, W.C. Jennings *et al.*, Phys. Rev. Lett. **56**, 1248 (1986).

[5] K. Matsuoka, S. Kubo, M. Hosokawa *et al.*, *Plasma Physics and Controlled Nuclear Fusion Research 1988* (*Proc. 12th Int. Conf.* Nice, 1988), IAEA, Vienna (1989) Vol. **2**, p.411.

[6] A. Fujisawa, H. Iguchi *et al.,* Rev. Sci. Instrum. **67**, 3099 (1996).

[7] A. Fujisawa, H. Iguchi *et al.,* Phys. Rev. Lett. **82**, 2669 (1999).

[8] A. Fujisawa, H. Iguchi *et al.,* Phys. Rev. Lett. **81**, 2256 (1998).

[9] K. Itoh and S.-I. Itoh, Plasma Phys. Control. Fusion **38**, 1 (1996).

[10] F. Wagner *et al.*, Phys. Rev. Lett. **49**, 1408 (1982).

[11] F.M. Levinton *et al.*, Phys. Rev. Lett. **75**, 4417 (1995).

[12] E.J. Strait *et al.*, Phys. Rev. Lett. **75**, 4421 (1995).

[13] S.-I. Itoh and K. Itoh, Phys. Rev. Lett. **60**, 2276 (1988).

[14] K.C. Shaing and E. Crume Jr., Phys. Rev. Lett. **63**, 2369 (1989).

[15] K. Itoh, S.-I. Itoh, A. Fukuyama, A. Sanuki and M. Yai, Plasma Phys. Control. Fusion **36**, 123 (1994).

[16] K.C. Shaing, Comments Plasma Phys. Control. Fusion **14**, 41 (1991).

[17] H. Biglari, P.H. Diamond and P.W. Terry, Phys. Fluids **2**, 1492 (1990).

[18] H. Zohm, F. Wagner *et al.,* Nucl. Fusion **32**, 489 (1992).

[19] S.-I. Itoh, K. Itoh, A. Fukuyama *et al.*, Phys. Rev. Lett. **28**, 2485 (1991).